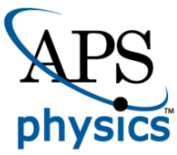

Application of a Magnetic Mirror to Increase Total Efficiency in Relativistic Magnetrons

Mikhail I. Fuks and Edl Schamiloglu

Phys. Rev. Lett. **122**, 224801 — Published 7 June 2019

DOI: 10.1103/PhysRevLett.122.224801

Application of a Magnetic Mirror to Increase Total Efficiency in Relativistic Magnetrons

Mikhail I. Fuks and Edl Schamiloglu*
Department of Electrical and Computer Engineering
University of New Mexico
Albuquerque, NM 87131-0001 USA
(Dated: May 13, 2019)

The relativistic magnetron is the most compact and efficient high-power microwave (HPM) source. In order to further increase the total efficiency of microwave generation in a relativistic magnetron with diffraction output (MDO) with a low energy state of electrons that is formed between two virtual cathodes (VCs) in the interaction space, the second VC at the downstream end of the interaction space is replaced with a magnetic mirror that reflects all leakage electrons back into the interaction space. Previously these leakage electrons were deposited on the anode surface without interacting with the microwaves. Particle-in-cell (PIC) simulations show that this configuration of relativistic magnetron increases the electronic efficiency from 86% to 92%, and increases the total efficiency up to the maximal electronic efficiency. This is a record high efficiency of microwave generation in a relativistic magnetron or any other gigawatt-class, gigahertz-frequency HPM source.

The invention of the cavity magnetron in 1940 and the subsequent development of radar and industrial applications are considered a "major innovation" according to the definition often used by technology historians [1]. Today, industrial cavity magnetrons abound and routinely operate reliably with beam-to-microwave conversion efficiencies exceeding 80%. The next big advance in the cavity magnetron was the relativistic magnetron that was first investigated by Bekefi and Orzechowski [2] and later by Palevsky and Bekefi at MIT in the late 1970s [3]. In these seminal works the authors achieved 900 MW in S-band with on the order of 20% beam-to-microwave conversion efficiency by extracting the radiation radially from one of 6 cavities. The relativistic magnetron came about following the advent of modern pulsed power in the 1960s [4], an electrical technology that led to the production of charged particle beams with currents in excess of 10 kA at voltages of 1 MV and more. These intense beams were applied to the simulation of nuclear weapons' effects, inertial confinement fusion, and other studies of high-energy density physics. The availability of intense relativistic electron beams allowed the knowledge of wave-particle interaction gained in the study of plasma physics to be put to use for the generation of HPM, with the relativistic magnetron being one such source.

In the first relativistic magnetron ([2]), the microwaves were extracted through a slot from one of the anode cavities. Such output provides for operation in the π-mode and its integer fractions. In [5, 6] the "magnetron with diffraction output" (MDO) was introduced, which is a relativistic magnetron in which all the cavities of its anode block are continued onto a conical output with gradually decreasing depth (Fig. 1). Unlike the relativistic magnetron with radial extraction [2, 3], the MDO can operate with any mode [7]. In order to improve MDO efficiency from that achieved in [5, 8] the dimensions were optimized [6].

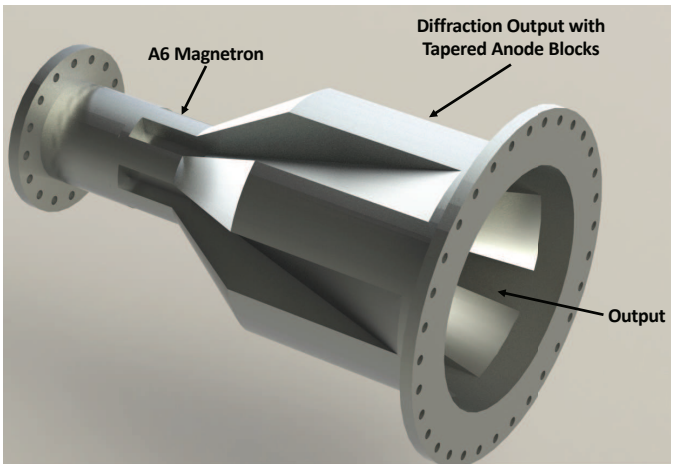

FIG. 1: Drawing of the University of New Mexico's S-band MDO.

In [9] it was shown using MAGIC PIC simulations [10] that when an electron beam is injected axially into the MDO, a low energy state of electrons with potential close to the potential of a physical cathode is realized between two virtual cathodes (VCs) (Fig. 2). Such VCs appear in a nonuniform channel consisting of three uniform drift tubes (Fig. 2 (top)). This channel is the interaction space of the MDO shown in Fig. 1 (labeled A6 Magnetron). The electron beam current is below the space-charge-limited current in the initial drift tube with radius $R_1 = 1.5$ cm. As the electron beam enters the second drift tube of radius $R_2 = 2.11$ cm (the interaction space), the beam current exceeds the space-charge-limited current and the first VC (VC1) appears (Fig. 2 (top, bottom)). The beam current following the first VC is Fedosov's current, given by [11]

$$I_{\rm F} = \frac{mc^3}{e}\frac{1}{2\ln\left(R_a/R_c\right)}\frac{(\gamma_a-\gamma_{\rm F})\sqrt{\gamma_{\rm F}^2-1}}{\gamma_{\rm F}}, \qquad (1)$$

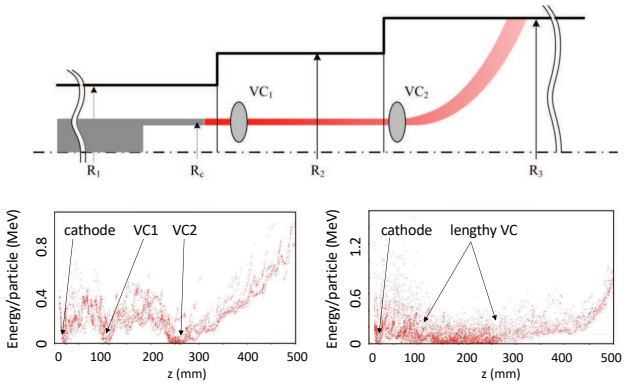

FIG. 2: Top: The MDO interaction region consisting of the three uniform drift tubes of progressively increasing radiii $R_1 < R_2 < R_3$. Bottom: Electron particles at 2 ns showing the formation of the two VCs (left) and the low energy state of electrons between the VCs (at 4 ns).

where $\gamma_a = 1 + eU_a/mc^2$, $\gamma_F = -0.5 + \sqrt{2\gamma_a + 0.25}$, m is the electron mass, e is the electron charge, c is the light speed, R_c is the cathode radius (1.0 cm), $R_a = R_2$ is the anode radius, U_a is the anode potential, and γ_a is the relativistic Lorentz factor. Fedosov's current is realized with a high energy state of electrons (Fig. 3) as for the case of a physical cathode [12].

The axial space-charge-limited current is given by [13]

$$I_{\rm lim} = \frac{mc^3}{e}\frac{1}{2\ln(R_a/R_c)}(\gamma_a^{2/3} - 1)^{3/2}. \qquad (2)$$

As the electron beam enters the output with radius $R_3 = 3.5$ cm (Fig. 3), it exceeds the space-charge-limited current and VC2 is formed, which partially suppresses the axial leakage current along tapered magnetic field lines.

In this Letter we introduce the use of a magnetic mirror at the output of the MDO instead of a second VC (VC2) to completely suppress axial leakage current. In PIC simulations we achieve 92% efficiency, which is a record for any gigawatt-class, gigahertz-frequency HPM source [13]. (It should be noted that Budker *et al.* had proposed that the gyrocon can generate 100s MW in the VHF band with efficiency that can approach 100% [14].)

Figure 4 shows the configuration of two MDOs. The one on top [9] is the variant with no physical cathode and two VCs, which gives the possibility of forming a low energy state of electrons in the interaction space with potential close to the potential that a physical cathode would be at. Absence of the physical cathode in the interaction space saves the cathode from electron bombardment and increases the lifetime of magnetrons. However, some leakage current $I_{\rm end}$ from the second VC, which deposits on the anode surface without interacting with microwaves (Fig. 4a), decreases the total efficiency

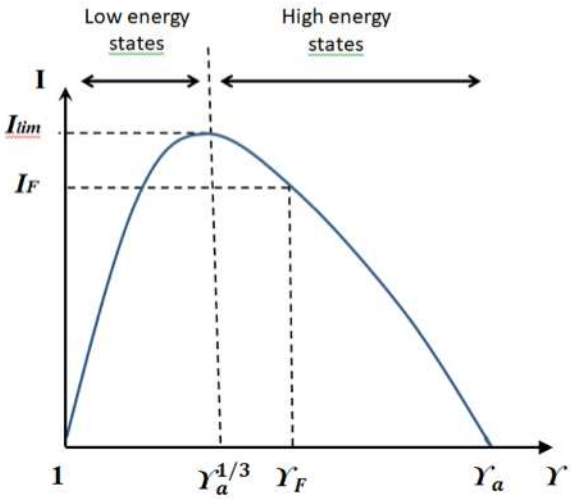

FIG. 3: Energy states of the beam electrons in the uniform channel. $I_{\rm lim}$ is the axial space-charge-limited current and $I_{\rm F}$ is the Fedosov current.

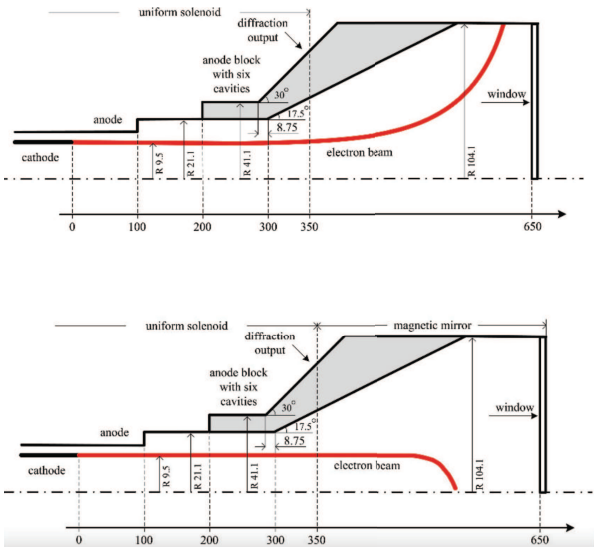

FIG. 4: Top: MDO dimensions (mm) with two VCs and the low energy state between them. The leakage current after the second VC deposits onto the anode. Bottom: The same MDO with a magnetic mirror instead of a second VC. The electron beam in red (color on-line) is shown in both cases.

$\eta = P/[U_a(I_a + I_{\rm end})]$ compared with the electronic efficiency $\eta_e = P/[U_a I_a]$. Here P is the output power and I_a is the anode current. It is pertinent to note that only the total efficiency is an objective indicator of device efficiency.

In order to increase the total efficiency to the electronic efficiency we propose to replace the second VC with an increasing magnetic field $H(z) = H_0[\exp(z - z_0)]^2$ where z_0 is the initial axial coordinate of the interaction space, in

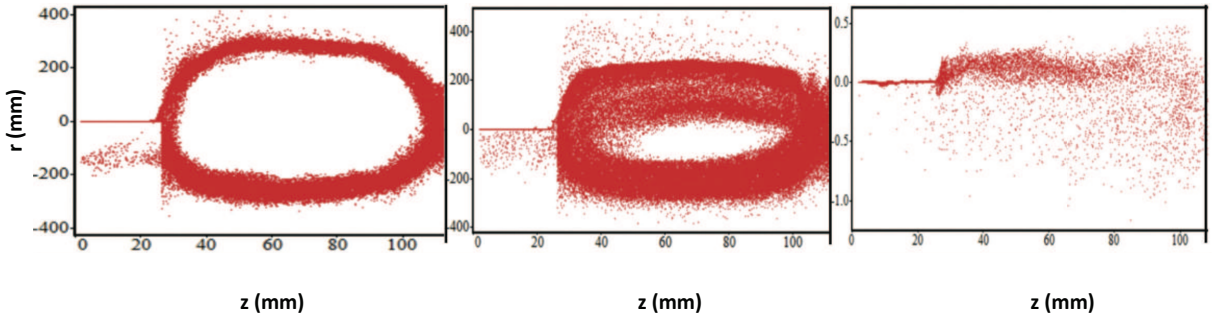

FIG. 5: Selective frames from MAGIC PIC simulations that demonstrate the temporal decrease of the longitudinal momentum of electrons in the MDO interaction space as the result of successive reflections from the magnetic mirror and the VC. (Note that the scale for the radius in the right plot is much finer than for the left and middle plots.) Left: at $t = 3$ ns; Middle: at $t = 6$ ns; Right: at $t = 12$ ns.

order to form a magnetic mirror at the output, which reflects all leakage electrons back into the interaction space and/or the VC. Following [15], the increasing magnetic field acts like a magnetic mirror which reflects all the electrons after VC_2 back into the interaction space. In order to reflect all electrons the total electron momentum

$$p = mc\gamma\beta \tag{3}$$

(here $\gamma = (1-\beta^2)^{-1/2}$, $\beta = v/c$, and v is the total electron velocity) can be represented as

$$p^2 = p_\perp^2 + p_\parallel^2 \tag{4}$$

where $p_\perp = mc\gamma\beta_\perp$, $\beta_\perp = v_\perp/c$, $v_\perp$ is the transverse velocity of electrons, $p_\parallel = mc\gamma\beta_\parallel$, $\beta_\parallel = v_\parallel/c$, and $v_\parallel$ is the longitudinal velocity of electrons. According to the first adiabatic invariant (μ) [16]

$$\mu = \frac{mv_\perp^2}{2B} = \text{constant}. \tag{5}$$

As the magnetic field B increases, the transverse momentum $p_\perp$ increases up to the total momentum

$$p_\perp = p \tag{6}$$

so that the longitudinal momentum decreases to

$$p_\parallel = 0 \tag{7}$$

when all electrons are reflected. Equation (5) or $v_\parallel = 0$ is the condition for reflection of electrons [16]. Let us assume $p_\perp > p$. Then from Eq. (2) it follows that $p_\parallel$ becomes imaginary, which is impossible for motion. Now the low energy state of electrons appears between the first VC and the magnetic mirror.

The dynamics of the establishment of the low energy state of the electron beam are complex. MAGIC simulations were performed with voltage $U = 400$ kV. A 1 ns risetime, 30 ns flat top waveform was used (the two available accelerators at the University of New Mexico to perform these experiments have pulselengths of 13 ns and 30 ns, respectively). Figure 5 presents selective frames from MAGIC PIC simulations that demonstrate the temporal

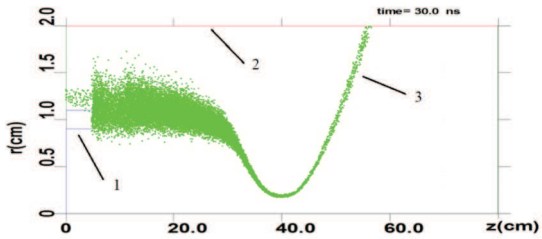

FIG. 6: Electrons penetrate through the magnetic mirror (3), drift towards the cathode external to the MDO interaction space (1) when $U_a = 400$ kV (between the anode (2) and the cathode (1)).

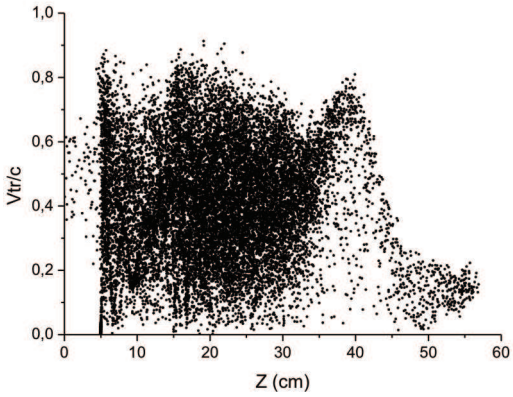

FIG. 7: Distribution of $v_\perp/c$ of electrons in the interaction space of the MDO as a function of axial position.

decrease of the longitudinal momentum of electrons in the MDO interaction space as a result of successive reflections between the magnetic mirror and the upstream VC. We postulate that the low energy state appears as follows. When all leakage electrons are reflected from the mirror and return to the VC these electrons are reflected from the plane of the VC plane where $v_\parallel = 0$. The elec-

tron space charge near the VC suppresses the current from the VC; however, the remaining current is added to the reflected electrons. Thus, the reflected electron beam becomes more dense and slower since its potential becomes lower. This scenario is repeated for each reflection. The results of multiple reflections is the establishment of the low energy state of electrons as in Fig. 5 that demonstrates the successive decrease of the longitudinal momentum $p_{\|}$ as a function of time t.

Note that, unlike the rapid establishment of the low energy state in a smooth channel as, for example, between two VCs [9], where electrons move only along the $z-$axis, in magnetrons it establishes slowly, during several 10s ns, because in magnetrons there is an anode current and those electrons give potential energy to microwaves. However, the presence of the anode current delays formation of the low energy state of electrons because, for reflections, such an anode current is clearly a loss current. Besides these evident losses there are some losses through the mirror and upstream to the cathode external to the MDO (Fig. 6). Computer simulations using the PIC code KARAT [17] show that the number of electrons with $p_{\perp} = 0$ are small (see Fig. 7). Such electrons do not satisfy the conditions of the adiabatic invariant, Eq. (3); therefore, they cannot satisfy $v_{\|} = 0$, which is a necessary condition for reflection.

On the positive part of the electron rings the longitudinal momentum of electrons is directed to $+z$, whereas on the negative part $p_{\|}$ is in the opposite direction. The left point where $p_{\|} = 0$ corresponds to reflection from the VC. The right point where $p_{\|} = 0$ corresponds to reflection from the magnetic mirror. PIC simulations show a magnetic field distribution given as $H(z) = H_0[\exp(z - z_0)]^2$, where H_0 is the uniform magnetic field in the MDO, $z > z_0$, and z_0 is the location where the uniform magnetic field in the interaction space ends and the increasing mirror magnetic field begins. Thus, a movable or immovable VC, together with a fixed magnetic mirror field can appear.

The movable VC drifts towards the fixed VC that appears near the entrance to the MDO from the tube connecting it to the cathode external to the MDO interaction space. Simulations show that after the VC interacts with the increasing magnetic field $H(z)$, a low energy state with a two-stream electron configuration appears as electrons are trapped between the VC and magnetic mirror, Fig. 8. Some electrons are able to drift towards the cathode external to the MDO interaction space, as seen in Fig. 8 between 0 and 10 cm. The electron beam incident into the MDO interaction space become denser with each reflection and the separation d between electrons decreases, which increases the impulsive force $F \simeq e^2/d^2$. Thus, the electron beam becomes thicker owing to the high electric field on the edge of the cathode emission area. As a result, part of the electrons pass over the cathode without reflection.

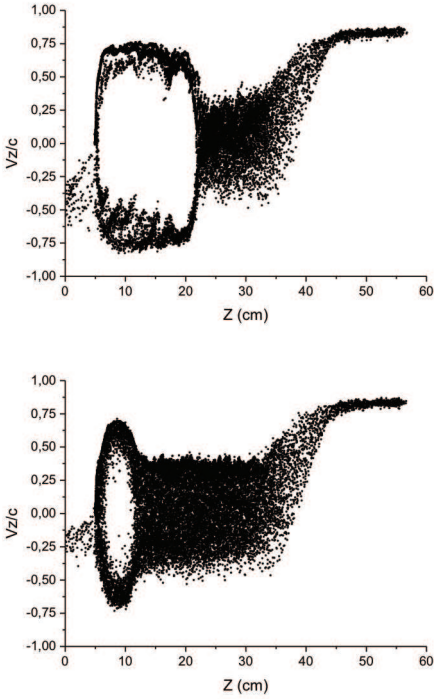

FIG. 8: Dependences of $p_{\|}$ on the longitudinal coordinate z at 5 ns (top) and 30 ns (bottom). The electron ring distributions are between the physical cathode (external to the MDO interaction space) and the VC, the low energy state is between the VC and the magnetic mirror.

In summary, PIC simulations have been used to show that replacing the downstream VC with a magnetic mirror in a relativistic MDO with no physical cathode (Fig. 1) leads to record high beam-to-microwave conversion efficiency in a gigawatt-class, gigahertz-frequency HPM source ranging from 86% to 92%. The total device efficiency reaches the maximal electronic efficiency.

This research was supported by ONR Grants N00014-16-1-2352 and N00014-19-1-2155. One of the authors (M.F.) wishes to thank M.B. Goykhman, A.V. Gromov, N.F. Kovalev, and 94 A.V. Palitsin (Institute of Applied Physics, Nizhny Novgorod, Russia) for useful discussions and performing the Karat simulations.

* edls@unm.edu

[1] Y. Blanchard, G. Galati, and P. van Genderen, IEEE Antennas Propag. Mag. **55**, 244 (2013).
[2] G. Bekefi and T. Orzechowski, Phys. Rev. Lett. **37**, 379 (1976).
[3] A. Palevsky and G. Bekefi, Phys. Fluids **22**, 986 (1979).
[4] E. Schamiloglu, R. Barker, M. Gundersen, and A. Neuber, Proc. IEEE **92**, 1014 (2004).
[5] N. Kovalev, B. Kol'chugin, V. Nechaev, M. Ofitserov, E. Soluyanov, and M. Fuks, Sov. Tech. Phys. Lett. **3**,

430 (1977).
[6] M. Fuks and E. Schamiloglu, IEEE Trans. Plasma Sci. **38**, 1302 (2010).
[7] M. Fuks, N. Kovalev, A. Andreev, and E. Schamiloglu, IEEE Trans. Plasma Sci. **34**, 620 (2006).
[8] M. Daimon and W. Jiang, Appl. Phys. Lett. **91**, 191503 (2007).
[9] M. Fuks, S. Prasad, and E. Schamiloglu, IEEE Trans. Plasma Sci. **44**, 1298 (2016).
[10] B. Goplen, L. Ludeking, D. Smithe, and G. Warren, Comp. Phys. Commun. **87**, 54 (1995).
[11] A. Fedosov, E. Litvinov, S. Belomytsev, and S. Bugaev, Sov. Phys. J. **20**, 1367 (1977).
[12] M. Fuks and E. Schamiloglu, Phys. Rev. Lett. **95**, 205101 (2005).
[13] J. Benford, J. Swegle, and E. Schamiloglu, *High Power Microwaves, 3rd. Ed.* (CRC Press, 2015).
[14] G. Budker, M. Karliner, I. Makarov, S. Morosov, O. Nezhevenko, G. Ostreiko, and I. Shekhtman, Part. Accel. **10**, 41 (1979).
[15] L. A. Artsimovich, *Controlled Thermonuclear Reactions* (Oliver and Boyd, 1964).
[16] F. Chen, *Introduction to Plasma Physics and Controlled Fusion* (Springer, 2016).
[17] N. Kovalev, Tech. Phys. **47**, 906 (2002).